

Laser-based measurement of parity violation in hydrogenC. Rasor  and D. C. Yost*Department of Physics, Colorado State University, Fort Collins, Colorado 80523, USA* (Received 27 November 2019; revised 10 July 2020; accepted 6 August 2020; published 1 September 2020)

A parity violation experiment based on stimulated emission in atomic hydrogen is analyzed. The intensity of a laser field within an optical cavity provides the experimental signal. We find that such a measurement would offer several advantages compared to previous experiments based on microwave spectroscopy, including a well-defined interaction region and a short coherent interaction time.

DOI: [10.1103/PhysRevA.102.032801](https://doi.org/10.1103/PhysRevA.102.032801)**I. INTRODUCTION**

Atomic parity violation (APV) provides a unique probe of electroweak theory at very low energies. At their core, such experiments measure the strength of the parity violating weak interaction between electrons and nucleons, which can be characterized by dimensionless nuclear spin-independent coupling constants C_{1p} and C_{1n} (electron-proton and electron-neutron coupling, respectively), and nuclear spin-dependent coupling constants C_{2p} and C_{2n} [1]. These constants relate to other weak interaction parameters such as the Weinberg mixing angle, $\sin^2\theta_W$, and the proton's weak charge, Q_W , which are determined through scattering experiments at higher energy [2–5]. A comparison between APV and scattering experiments provides an excellent test of the running of the Weinberg angle. While APV experiments typically probe transitions at the ~ 1 eV energy region, they are sensitive to beyond-Standard-Model physics, and they set limits on possible new particles at the TeV scale [6]. For example, a precise measurement of $\sin^2\theta_W$ at low momentum transfer would help facilitate the search for the dark Z boson [7].

In 1974, Bouchiat and Bouchiat analyzed possible parity violating effects in heavy atoms, and they found that the parity violating amplitude grows faster than Z^3 , where Z is the atomic number [8]. Numerous successful heavy-atom APV experiments have been performed since [9–18]. To date, the Boulder cesium experiment remains the most precise APV experiment, resulting in the only observation of an anapole moment [15].

However, the argument in favor of heavy-atom APV is more nuanced than it initially appears. Hydrogen, with its nearly degenerate states of opposite parity, produces APV amplitudes that are similar in magnitude to those of cesium. In addition, experiments in hydrogen and deuterium offer several other attractive features—the four electron/nucleon coupling constants can be experimentally isolated by performing measurements of hydrogen and deuterium at several magnetic fields, and the required atomic physics calculations can be performed with high accuracy. This can be compared with cesium, where sophisticated atomic and nuclear structure calculations are necessary to extract $\sin^2\theta_w$, which have been continually refined over the past 20 years [6,19].

Interest in hydrogen APV experiments began even before the advent of the Glashow-Weinberg-Salam theory of electroweak interactions [20,21]. By the early 1980s, three groups—at Michigan, Washington, and Yale—had started experiments to measure such effects within the $n = 2$ manifold of hydrogen using microwave spectroscopy and fast atomic beams [22–24]. Although the limits slowly improved, none of the experiments were successful in observing parity violation, and all were eventually abandoned. In 2007, Dunford and Holt proposed another APV measurement in hydrogen, also using microwave transitions within the hydrogen $n = 2$ state; their scheme utilizes a thermal beam of hydrogen at 77 K and they discuss methods to mitigate the systematic effects from stray electric fields [25].

The aim of this article is to provide analysis for a laser-based hydrogen APV measurement. Considering previous hydrogen APV measurements were limited by stray electric fields, laser-based measurements have the advantage that interaction regions are very well-defined and can be made far away from surfaces. In terms of such measurements, there has only been one proposed—the absorption of circularly polarized light between the $2s$ - $3s$ states [26]. Here, we analyze a laser-based scheme based on stimulated emission, and we conclude that it would be far superior in terms of signal-to-noise compared to the previously proposed absorption measurement, and it deserves close consideration.

II. GENERAL CONSIDERATIONS

The measurement we consider would be performed within a static magnetic field. Michel was the first to suggest that by performing a hydrogen parity nonconservation measurement in a static magnetic field, opposite parity states can be made to cross, which will increase the parity nonconserving amplitude, A_{pnc} [21]. For the laser-based experiment we consider here, this will increase the statistical signal to noise. In addition, the use of a magnetic field also allows one to isolate contributions from nuclear-spin-dependent and nuclear-spin-independent coupling constants. The Zeeman splitting of the hydrogen $n = 2$ and 3 manifolds is shown in Fig. 1. We use

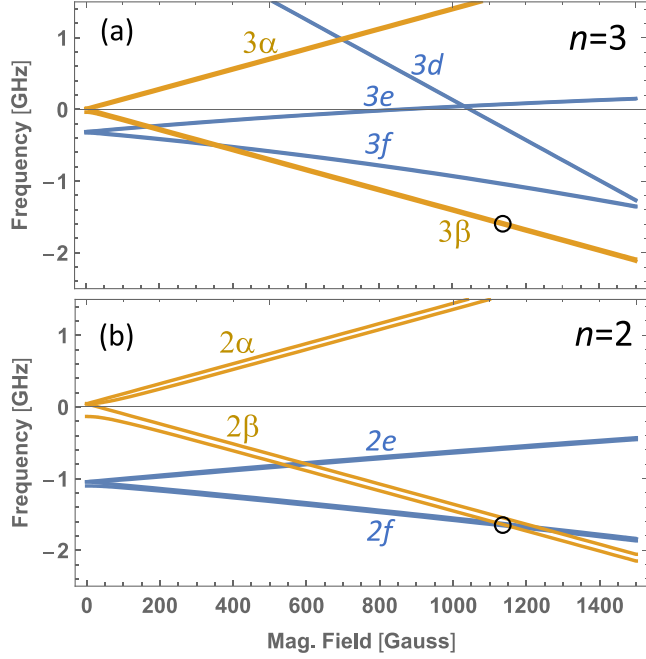


FIG. 1. Zeeman splitting of hydrogen within (a) the $n = 3$ manifold and (b) the $n = 2$ manifold. The position of the level crossing near 1200 G is shown in both figures, and the frequency axes are with respect to the $3s$ and $2s$ hyperfine centroids, respectively. Lamb's notation is used to represent the fine structure. Hyperfine levels are included in both plots, but the splitting is too small to observe in (a).

Lamb's notation [27] to describe the fine structure within both manifolds with subscripts indicating the m_F quantum number.

While level crossings occur near both 550 and 1200 G, we will focus on the level crossing between $|2\beta_0\rangle$ and $|2f_0\rangle$, but note that the same analysis can be applied to $|2\beta_0\rangle$ and $|2e_0\rangle$. Figure 2 shows the level crossing region in more detail. Because the weak interaction conserves the m_F quantum number, the relevant weak-induced Rabi frequencies near this level crossing are

$$\frac{\langle 2f_0|U_w|2\beta_0\rangle}{\hbar} = i\bar{V}(C_{1p} + 1.1C_{2p}) \approx 7i \times 10^{-3} \text{ s}^{-1},$$

$$\frac{\langle 2f_{-1}|U_w|2\beta_{-1}\rangle}{\hbar} = i\bar{V}(C_{1p} - C_{2p}) \approx -6i \times 10^{-4} \text{ s}^{-1},$$

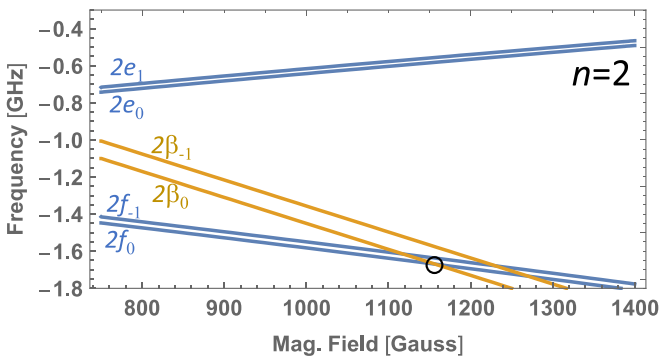


FIG. 2. Zeeman splitting of hydrogen within the $n = 2$ manifold near the level crossing around 1200 G. The subscripts indicate m_F .

where U_w is the parity nonconserving weak energy, \bar{V} is the APV coupling strength (given by ≈ 0.013 Hz for $n = 2$), and the numerical values are the approximate Standard Model predictions [1,25]. Since it is about one order of magnitude larger, we will concentrate on the $\langle 2f_0|U_w|2\beta_0\rangle$ matrix element and define Ω_w as

$$\Omega_w = \frac{\langle 2f_0|U_w|2\beta_0\rangle}{\hbar},$$

where it is important to note that this Rabi frequency is purely imaginary.

Before investigating our laser-based method to measure Ω_w , we will first consider an early and simple proposal given in [21]. At the level crossing, the weak interaction will mix the metastable $|2\beta_0\rangle$ with $|2f_0\rangle$, inducing decay back to the hydrogen ground state, emitting a Lyman- α photon. The number of decays from $|2\beta_0\rangle$ due to the weak interaction is given by $4|\Omega_w|^2/\gamma_{2p} \approx 3 \times 10^{-13}/\text{s}$, where γ_{2p} is the decay rate from $|2f_0\rangle$. Therefore, a measurement of this decay rate performed by detection of the resulting Lyman- α photons effectively measures the weak interaction.

From a purely statistical vantage point, a measurement of this sort appears possible. While the decay rate is extremely small, a beam-type experiment with 10^{10} $|2\beta_0\rangle$ atoms within the measurement volume would produce count rates of 0.003 Hz. A 10% measurement of Ω_w would require only a few hours of data collection. Of course, the challenge, which was also recognized by Michel [21], is that it would seem to be nearly impossible to differentiate these decays from the large background that would also be produced. Two-photon decays out of the $2S$ state occur at a rate that is about 13 orders of magnitude larger than the rate due to weak interactions, and collision-induced decays would likely be even larger.

To produce signals that are larger than the background, one typically aims to interfere A_{pnc} —given in the last example by the steady-state amplitude in the $|2f_0\rangle$ due to the weak interaction, $2\Omega_w/\gamma_{2p}$ —with some larger parity conserving amplitude, A_{pc} . With this, the total transition rate is proportional to

$$|A_{\text{pc}} + A_{\text{pnc}}|^2 = |A_{\text{pc}}|^2 + 2|A_{\text{pc}}||A_{\text{pnc}}|\cos\phi + |A_{\text{pnc}}|^2,$$

where ϕ is the phase between A_{pc} and A_{pnc} . The last term, $|A_{\text{pnc}}|^2$, is very small and will be dropped going forward, and the sign of the cross term depends on the handedness of the apparatus, which is inverted by adjusting ϕ by π . The count rate will then be given by

$$R_{\pm} = \eta N_a \gamma_{2p} (|A_{\text{pc}}|^2 \pm 2|A_{\text{pc}}||A_{\text{pnc}}|),$$

where N_a is the number of atoms within the measurement volume, and η is the detection efficiency. Since the value of A_{pc} can be controlled in a laboratory setting, it can be increased until the second A_{pnc} -dependent term is larger than the background. However, as discussed in [23], A_{pc} should not be made too large, or systematic effects associated with A_{pc} itself may become problematic.

During a typical measurement, the handedness of the apparatus is reversed and the results subtracted to isolate the A_{pnc} -dependent term. With this, the shot-noise limited signal-

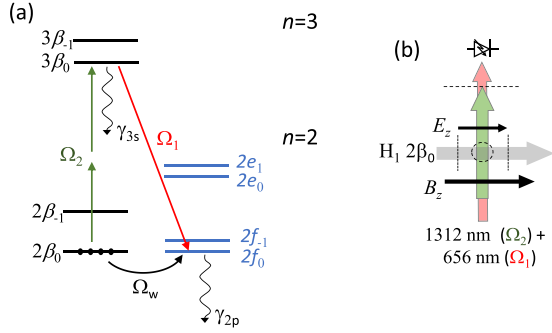


FIG. 3. Measurement scheme to introduce a parity conserving amplitude that interferes with Ω_w at the $|2f_0\rangle$ state. (a) The energy levels of interest along with relevant fields driving the transitions. (b) Schematic of the applied fields within the interaction volume; the atomic beam is traveling along the direction of the magnetic field, B_z . An applied electric field, E_z , will be parallel or antiparallel to the atomic beam. The two laser fields are collinear and propagating transverse to the atom beam.

to-noise ratio is given by

$$\text{SNR} = \frac{\frac{1}{2}(R_+ - R_-)\tau}{\sqrt{\frac{1}{2}(R_+ + R_-)\tau}} = 2\sqrt{\eta N_a \tau \gamma_{2p} A_{\text{pnc}}}, \quad (5)$$

where τ is the total measurement time. We obtain the familiar result that simply introducing a parity conserving amplitude, A_{pc} , neither improves nor degrades the statistical signal-to-noise ratio. Therefore, a good baseline for the SNR achievable in a generic APV measurement based within the hydrogen $n = 2$ manifold is found by setting A_{pnc} to the amplitude given in the simple example above. Doing so provides the SNR given by

$$\text{SNR}_b = 4 \Omega_w \sqrt{\frac{\eta N_a \tau}{\gamma_{2p}}}. \quad (6)$$

In evaluating our laser-based stimulated emission experiment, which is the focus of this article, we find it helpful to compare with this baseline SNR.

III. MEASUREMENT BASED ON STIMULATED EMISSION

As discussed in the previous section, a simple measurement based on weak-induced decays of hydrogen from the $|2\beta_0\rangle$ state would be impossible due to the large background. Therefore, the introduction of a parity conserving amplitude is necessary. Unfortunately, a simple DC electric field used to Stark-mix the $|2\beta_0\rangle$ and $|2f_0\rangle$ states will not produce the desired interference since Ω_w will be imaginary whereas the Stark amplitude will be real [26].

Therefore, we consider producing the parity conserving amplitude by driving the $2S$ - $3S$ two-photon transition at 1312 nm with Rabi frequency Ω_2 [28], along with the $3S$ - $2P$ transition at 656 nm with Rabi frequency Ω_1 . For the upper level, we choose the $|3\beta_0\rangle$ state since it has, by far, the largest two-photon transition probability when starting at $|2\beta_0\rangle$. The relevant levels associated with this scheme are shown in Fig. 3. Constructive or destructive interference between A_{pnc}

and A_{pc} is possible by adjusting the relative phase between the two laser fields in a manner similar to that shown in [29].

This measurement scheme offers an attractive way to detect Ω_w that does not rely on the measurement of Lyman- α photons, but instead would aim to detect the stimulated emission from $|3\beta_0\rangle$ to $|2f_0\rangle$, which mitigates the large background further. Measurements of APV using stimulated emission to increase detector efficiency have previously been used in [16].

To analyze this measurement scheme, we start with the Lindblad form of the master equation, which describes the time evolution of the density matrix of our system,

$$\partial_t \rho = -\frac{i}{\hbar}[H, \rho] + \Gamma \mathcal{L}[\sigma], \quad (7)$$

where Γ is the spontaneous emission rate of each relevant state (γ_{2p} for $|2f_0\rangle$ and γ_{3s} for $|3\beta_0\rangle$) and $\mathcal{L}[\sigma]$ is the Lindblad superoperator defined as

$$\mathcal{L}[\sigma] = \sigma \rho \sigma^\dagger - \frac{1}{2}(\sigma^\dagger \sigma \rho + \rho \sigma^\dagger \sigma), \quad (8)$$

with $\sigma_{ij} = |i\rangle\langle j|$ being the atomic lowering operator. The Hamiltonian is comprised of state energies, H_k , and interaction terms in the rotating wave approximation, $H = H_k + H_1 + H_2 + H_w$ [25,28,30]:

$$\begin{aligned} H_k &= \hbar \omega_k \sigma_{kk}, \\ H_1 &= \hbar \frac{\Omega_1}{2} (\sigma_{f3} e^{i\phi} + \sigma_{f3}^\dagger e^{-i\phi}), \\ H_2 &= \hbar \frac{\Omega_2}{2} (\sigma_{\beta 3} + \sigma_{\beta 3}^\dagger), \\ H_w &= \hbar (\Omega_w \sigma_{f\beta} + \Omega_w^* \sigma_{f\beta}^\dagger), \end{aligned} \quad (9)$$

where ϕ is the relative phase between the one-photon and two-photon laser fields.

We consider the limit of weak excitation in which $\gamma \gg \Omega$ for all transitions, and we assume that the system is initially in $|2\beta_0\rangle$. Allowing population to transfer out of the $|2\beta_0\rangle$ state at the damped Rabi rate, $\partial_t \sigma_{\beta\beta} = 4\Omega_2^2/\gamma_{3s}$, we can solve the system of density matrix equations for the otherwise steady-state single-photon coherence term ρ_{f3} . Doing so, we find

$$\rho_{f3} = \frac{\Omega_1 \Omega_2^2}{\gamma_{3s}^2 \gamma_{2p}} e^{i\phi} + \frac{2|\Omega_w| \Omega_2}{\gamma_{3s} \gamma_{2p}}. \quad (10)$$

Using this coherence term, the gain coefficient, $\Gamma^{(g)}$, of the single-photon laser field propagating through the atomic medium can then be obtained by combining both the susceptibility relation shown in [31], $\epsilon_0 E_0 \chi'' = 2N \mu_{f3} \text{Im}(\rho_{f3} e^{-i\phi})$, and the single pass gain equation, $\Gamma^{(g)} = -\omega l \chi''/c$, described in [32]. Here, ϵ_0 is the vacuum permittivity, E_0 is the electric field of the laser, N is the number of atoms in the interaction region, μ_{f3} is the dipole matrix element between the $|3\beta_0\rangle$ and $|2f_0\rangle$ states, and l is the length of the gain medium. The gain coefficient is calculated to be

$$\Gamma^{(g)} = \frac{n_a}{\Phi} \left(\frac{\Omega_1^2 \Omega_2^2}{\gamma_{3s}^2 \gamma_{2p}} + \frac{2|\Omega_w| \Omega_1 \Omega_2}{\gamma_{3s} \gamma_{2p}} \cos \phi \right), \quad (11)$$

where Φ is the photon flux associated with Ω_1 , n_a is the atomic density, and we have dropped the very small term proportional to $|\Omega_w|^2$. To simplify the notation, we introduce $\Gamma_0^{(g)}$ and $\Gamma_w^{(g)}$

through

$$\Gamma^{(g)} = \Gamma_0^{(g)} + \Gamma_w^{(g)} \cos \phi. \quad (12)$$

From this expression, we note that the single pass gain through the medium will be given approximately by the $\Gamma_0^{(g)}$ value with only a small modulation due to $\Gamma_w^{(g)}$. The reversal of the handedness of the apparatus is accomplished by incrementing ϕ by π . This can be understood intuitively since a laser field superimposed with its second harmonic defines a preferred direction in space depending on the relative phase of the two fields. Whether this direction is parallel or antiparallel to the magnetic field defines the handedness.

The larger gain coefficient, $\Gamma_0^{(g)}$, can be varied experimentally through the two-photon Rabi frequency Ω_2 . Since $\Gamma_0^{(g)}$ is the more experimentally relevant quantity, it is helpful to frame the problem entirely in terms of that coefficient. Doing so, $\Gamma_w^{(g)}$ can be written as

$$\Gamma_w^{(g)} = 2 \sqrt{\frac{n_a \Gamma_0^{(g)}}{\Phi \gamma_{2p}}} |\Omega_w|. \quad (13)$$

To calculate the SNR for this measurement scheme, we first solve for the photon flux at the output of the measurement volume, which is taken to have a length l . This is done by solving the differential gain equation, $d\Phi/dl = \Gamma^{(g)}\Phi$. The result is

$$\Phi(l) = \Phi(0)e^{\Gamma_0^{(g)}l} + 4 \sqrt{\frac{\Phi(0)n_a}{\Gamma_0^{(g)}\gamma_{2p}}} |\Omega_w| \left(e^{\Gamma_0^{(g)}l} - e^{\frac{\Gamma_0^{(g)}l}{2}} \right) \cos \phi. \quad (14)$$

Then, we replace R_{\pm} in Eq. (5) with the photon detection rate, given by $\Phi(l)\eta A$, where A is the area of the laser beam. The result is

$$\text{SNR}_e = \text{SNR}_b \frac{e^{\frac{\Gamma_0^{(g)}l}{2}} - 1}{\sqrt{\Gamma_0^{(g)}l}}. \quad (15)$$

This expression almost reproduces our baseline estimate of the signal to noise discussed earlier—but with an extra expression related to the total photon gain through the atomic medium. The baseline expression is recovered for $\Gamma_0^{(g)}l \approx 1.65$. However, we emphasize that this expression is not valid for $\Gamma_0^{(g)}l$ much greater than 1 due to saturation effects that have been ignored in this analysis.

The previous analysis indicates that $\Gamma_0^{(g)}l \approx 1$ is desirable from a statistical perspective. However, for technical reasons this may be difficult to achieve in practice. For instance, we can consider a thermal beam of $|2\beta_0\rangle$ atoms, a centimeter-scale interaction volume, a metastable density of $3 \times 10^9 \text{ cm}^{-3}$ (density limits for a 30 cm mean free path, given in [25]), and weak excitation from $|2\beta_0\rangle$ to $|3\beta_0\rangle$. For these experimentally reasonable values, an estimate gives $\Gamma_0^{(g)}l \sim 0.03$, which would severely degrade the SNR according to Eq. (15). Therefore, we now consider $\Gamma_0^{(g)}l \ll 1$ along with the addition of an optical cavity to enhance the field associated with Ω_1 , as shown in Fig. 4. This effectively increases the interaction length of the medium by the power buildup of the cavity. Given the modest increase in interaction

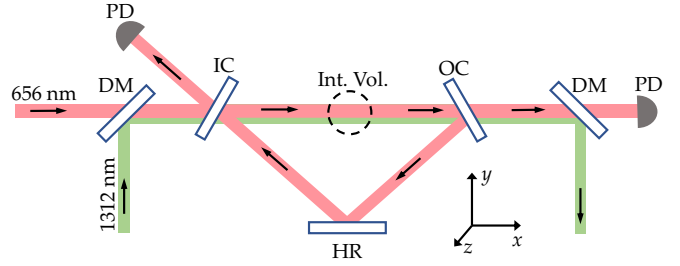


FIG. 4. Schematic of the experimental setup; metastable hydrogen atoms travel through the interaction volume (Int. Vol.) along the z -direction. The 656 nm field is built up in a low finesse cavity comprised of an input coupler (IC), an output coupler (OC), and a high reflector (HR). Dichroic mirrors (DC) are used to overlap the two laser fields entering the cavity, then separate the fields before detection onto a photodiode (PD). The 656 nm light provides the measurement signal of the stimulated emission generated from $|3\beta_0\rangle$ to $|2f_0\rangle$. Both lasers would be polarized in the z -direction, and the relative phase would be varied to produce constructive or destructive interference at $|2f_0\rangle$, isolating Ω_w . Electric field plates will also be present to control the field within the interaction volume, but they are excluded from the diagram for clarity.

length required, a buildup of 100 is likely sufficient. To have a well-defined phase between the 1312 and 656 nm fields, it would be necessary to build the 656 nm buildup cavity as a ring cavity so that the two fields are copropagating.

To analyze this case, we assume the optical cavity has an input and an output coupler both with transmission T . With such low cavity finesse, we can assume that all cavity loss is through mirror transmission, and the relationship between the photon flux incident on a cavity Φ_{in} and the photon flux transmitted Φ_{out} is then given in the semiclassical approximation by

$$\begin{aligned} \frac{\Phi_{\text{out}}}{\Phi_{\text{in}}} &= \frac{1}{\left(1 - \frac{\Gamma^{(g)}l}{2T}\right)^2} \\ &\approx \frac{1}{(1 - \alpha^{(g)})^2} - \frac{\Gamma^{(g)}l}{T} \frac{\cos \phi}{(1 - \alpha^{(g)})^3}, \end{aligned} \quad (16)$$

where $\alpha^{(g)} = \Gamma_0^{(g)}l/(2T)$. In this case, the experimental setup resembles an injected laser below threshold. The dimensionless parameter $\alpha^{(g)}$ can be thought of as determining the system's proximity to the lasing threshold.

From the last expression, we can calculate the statistical SNR with the addition of an optical cavity, which is given by

$$\text{SNR}_e^{\text{cav}} = \text{SNR}_b \frac{\sqrt{\alpha^{(g)}}}{\sqrt{2}(1 - \alpha^{(g)})}. \quad (17)$$

This nearly reproduces our previous baseline SNR estimates where exact agreement is obtained if $\alpha^{(g)}$ is set to 1/2. Similar to Eq. (15), this result is only valid for $\alpha^{(g)}$ slightly less than 1/2 due to saturation effects being ignored. Nevertheless, this result shows that the SNR using a laser-based measurement could approach SNR_b , while effectively eliminating the background inherent in a fluorescence measurement.

Within this measurement scheme, A_{pc} is effectively controlled through the strengths of the 1312 and 656 nm laser fields. As discussed earlier, A_{pc} should not be made too large

or else systematic effects related to A_{pc} itself may become problematic. To quantify this, one can consider the asymmetry, \mathcal{A} , the ratio of differential signal obtained after a reversal to the total signal, given by $2A_{pnc}/A_{pc}$. Typical values for asymmetry in APV measurements are usually on the order of 10^{-6} . Considering our proposed scheme, the asymmetry in photon counts is given by

$$\mathcal{A} = \frac{R_+ - R_-}{R_+ + R_-} = \frac{\text{SNR}}{\sqrt{N_p \eta}}, \quad (18)$$

where N_p is the total photon count incident on the detector within a given integration time. For a simple estimate, if $\text{SNR} \sim 1$ for $\tau = 1$ s then to maintain $2A_{pnc}/A_{pc} > 10^{-6}$ the total power incident on the photodiode should be $< 1 \mu\text{W}$. This shows that a likely experimental realization will use 656 nm laser power, which is small but not unreasonable.

IV. DISCUSSION

A. Advantages of the laser-based measurement

Our main result, as shown in Eq. (17), is that our proposed measurement has a statistical signal-to-noise that can approach SNR_b . However, the microwave experiments previously conducted and proposed were also designed to approach SNR_b . Therefore, this is not the main motivation. Instead, we believe there are advantages in reduced susceptibility to systematic effects, and low requirements on the coherence of the interaction. These two points are discussed in the following subsections.

1. Systematic effects

Past hydrogen APV measurements performed well in terms of statistical SNR, but faced serious systematic effects. The most important systematic was due to stray electric fields and/or motional electric fields [33–35]. One of the strongest cases in favor of laser-based measurements is that the interaction volume is very localized and can be made far away from surfaces. This was significantly more challenging for the past microwave-based measurements.

The problems of stray field systematics in hydrogen APV stem from the near degeneracy of opposite parity states. A static electric field in the z direction of only ~ 5 nV/cm produces a Rabi frequency, $\Omega_{Ez}^{f_0}$, between $|2\beta_0\rangle$ and $|2f_0\rangle$ [as depicted in Fig. 5(d)] with the same magnitude as Ω_w . However, it is incorrect to insist that electric fields be controlled at this level since Ω_w is imaginary and its effects can, therefore, be differentiated. In fact, a small variable field applied in the z -direction would allow one to calibrate the size of Ω_w while continuously varying the relative phase of Ω_1 and Ω_2 in a manner similar to that demonstrated in [29]. The near perfect reversal that can be obtained through the continuous adjustment of the relative phase between two laser fields is a major advantage of this style of laser-based measurements.

In addition to the coupling at $|2f_0\rangle$, a stray electric field in the z -direction will also couple $|2\beta_0\rangle$ to $|2e_0\rangle$. The 656 nm light can then drive the $|3\beta_0\rangle \rightarrow |2f_0\rangle$ transition, creating an interference that mimics our PNC signal, shown in Fig. 5(b). This signal is mitigated, however, by the small dipole moments that exist between the pairs of states, as well as by the

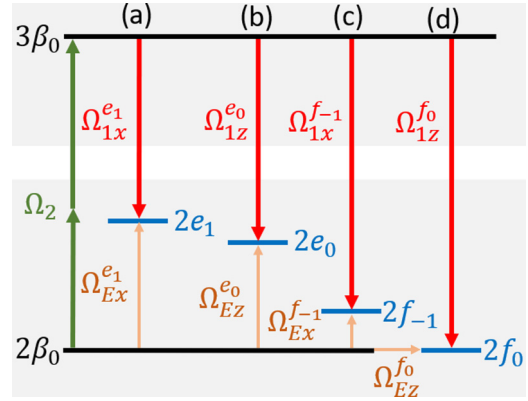


FIG. 5. Possible transitions due to systematics such as stray electric fields, laser misalignment, and polarization mismatching. (a),(c) Stray electric fields in the x -direction and x -polarized 656 nm light. (b),(d) Stray electric fields in the z -direction and z -polarized 656 nm light.

≈ 1 GHz off resonance of the $|2e_0\rangle$ state. Further mitigation occurs when the aforementioned variable electric field is applied to calibrate Ω_w . Whenever $|2f_0\rangle$ is driven with E_z at the same Rabi rate as Ω_w , the signal due to the $|2e_0\rangle$ interference is about 10^4 times smaller than that of the PNC signal.

More problematic would be stray electric fields orthogonal to the applied magnetic field, which would couple $|2\beta_0\rangle$ and $|2e_1\rangle$, as in Fig. 5(a). This amplitude would produce an interference signal by allowing the 656 nm field to then drive the $|3\beta_0\rangle \rightarrow |2e_1\rangle$ transition, which could imitate the Ω_w interference at $|2f_0\rangle$. However, this spurious interference signal would be suppressed by two orders of magnitude because of the ≈ 1 GHz detuning factor gained between $|2\beta_0\rangle$ and $|2e_1\rangle$. Additional suppression occurs by ensuring the 656 nm field is z -polarized with respect to the applied B_z field. Such a polarization alignment could likely be performed to an accuracy of $\sim 10^{-4}$ or better.

Similar mixing can occur through the $|2\beta_0\rangle$ and $|2f_{-1}\rangle$ state due to orthogonal stray electric fields, along with the transition between $|2f_{-1}\rangle$ and $|3\beta_0\rangle$ by near-resonant x - or y -polarized 656 nm light [see Fig. 5(c)]. Again, this spurious interference effect is suppressed through polarization control of the 656 nm light, and is further mitigated by the nature of small dipole moments between these states.

Since each of the $2P_{1/2}$ sublevels can potentially carry an interference signal due to stray electric fields, we examine the relative signal size in terms of photon flux out of the cavity, compared to the weak result in Eq. (16). Performing the same analysis as described in Sec. III, but including a static electric field and off-resonant $2P_{1/2}$ states, we solve for the oscillating term of the cavity output photon flux, Φ_E , due to an electric field, and we compare to the oscillating term of the weak cavity output flux, Φ_W . Adding in quadrature electric field contributions that are in-phase and out-of-phase with the weak interaction places an upper limit of systematic flux in the form of

$$\frac{\Phi_E}{\Phi_W} \approx \frac{\Omega_1^{2P} \Omega_E^{2P}}{|\Omega_{1z}^{f_0}| |\Omega_W|} \frac{\tilde{\alpha}^{(g)}}{\sqrt{1 + (2\Delta\omega/\gamma_{2P})^2}}, \quad (19)$$

TABLE I. Relative photon flux due to stray electric fields compared to that of PNC effects using Eq. (19). The assumed stray fields are expected upper limits on both the longitudinal and transverse directions. We assume a polarization purity of 10^4 in the z -direction. The ratio $\Omega_1^{2P}/\Omega_{1z}^{f0}$ is the ratio of single-photon Rabi rates from the upper $|3\beta_0\rangle$ state to each of the $2P_{1/2}$ states, $2P = \{2e_1, 2e_0, 2f_{-1}, 2f_0\}$. The ratio Ω_E^{2P}/Ω_W compares Rabi rates of Stark mixing due to stray electric fields at the different $2P_{1/2}$ states to the Rabi rate due to weak mixing. The term $\tilde{\alpha}$ describes the relative lasing thresholds of the medium due to weak interaction compared to stray electric field interactions. We note in the last column whether each systematic is in- or out-of-phase with the weak Rabi rate, Ω_w . The leading systematic, caused by $|2f_0\rangle$, is out-of-phase with Ω_w , which further suppresses its effects, as discussed in Sec. IV A 2 of the text. The (a) and (c) systematics due to the presence of an x -direction electric field arise from spurious polarization of the 656 nm field, and thus cannot be said to have a defined phase with the weak amplitude. For our calculations, we assume these amplitudes to be in-phase with the weak rate. Therefore, the values listed here represent upper limits but would likely be further suppressed.

	$2P_{1/2}$ sublevel	Stray \vec{E} field	Polarization suppression	$\Omega_1^{2P}/\Omega_{1z}^{f0}$	Ω_E^{2P}/Ω_W	$\Delta\omega/2\pi$ (MHz)	$\tilde{\alpha}^{(g)}$	Φ_E/Φ_W	Relative phase to Ω_w
(a)	$2e_1$	$30 \mu\text{V}/\text{cm} \hat{x}$	10^4	9.5×10^{-5}	5.7×10^4	1114	1/8	3.0×10^{-3}	und.
(b)	$2e_0$	$5 \text{nV}/\text{cm} \hat{z}$	1	0.034	0.05	1085	1/8	9.8×10^{-6}	0
(c)	$2f_{-1}$	$30 \mu\text{V}/\text{cm} \hat{x}$	10^4	6.9×10^{-7}	140	30	1/8	1.0×10^{-5}	und.
(d)	$2f_0$	$5 \text{nV}/\text{cm} \hat{z}$	1	1	1	0	1	1	$\pi/2$

where Ω_1^{2P} is the one-photon Rabi rate between the $|3\beta_0\rangle$ state and respective $2P_{1/2}$ states ($|2e_0\rangle, |2e_1\rangle, |2f_{-1}\rangle, |2f_0\rangle$), Ω_E^{2P} is the Rabi rate due to static electric fields, and $\Delta\omega$ is the frequency detuning of the laser to the corresponding sublevel. The term $\tilde{\alpha}^{(g)} = (1 - \alpha_w^{(g)})^3 / (1 - \alpha_E^{(g)})^3$ is related to the relative lasing thresholds of the gain medium due to the respective weak interaction and to the stray electric fields. In this case, we set $\alpha^{(g)} = 1/2$, which implies $\alpha_E^{(g)} \ll \alpha_w^{(g)}$ for $2P_{1/2}$ sublevels (a), (b), and (c). For each of the sublevels, we have tabulated the ratio of extraneous systematic photon flux to the photon flux due to the PNC effect using experimentally realizable limits, which demonstrates that the systematic effects are significantly suppressed in this experiment. Table I displays the results of Eq. (19), where we assume stray electric field amplitudes in both the x - and z -directions of $30 \mu\text{V}/\text{cm}$ and $5 \text{nV}/\text{cm}$, respectively, and a polarization purity of the 656 nm laser of 10^4 .

2. Systematic effects mitigation

In this section, we demonstrate how the small stray fields shown in Table I can be achieved experimentally, as well as showing how a carefully devised measurement scheme can be made relatively insensitive to the stray-field systematic effects. Finally, we support these conclusions with an illustrative simulation that implements a drifting E_z field, showing that the weak induced signal can still be reliably extracted.

To justify the assumptions of the small orthogonal stray electric fields in the previous section, we consider rotating the polarization of the 656 nm field by 90° and measuring the greatly amplified interference signal at $|2e_1\rangle$. This polarization rotation can be very accurately performed since within a ring cavity s - and p -polarization are nondegenerate and thus the cavity naturally behaves as a polarization filter. In 1 s of collection time, this system would be sensitive to detecting fields down to $\sim 30 \mu\text{V}/\text{cm}$, which is comparable to the $\mu\text{V}/\text{cm}$ levels of detection achieved in krypton atoms by [36]. By tuning additional electric field plates, the stray fields can be minimized, and polarization of the 656 nm field can be rotated back to the z -direction for the PNC measurement, similar to the method in [15].

One complication to consider is the motional electric fields that would be present if the atomic beam is not precisely aligned to the applied magnetic field, demonstrating the advantages of a cold atomic beam with a small divergence [25]. Given a thermal beam of hydrogen with an average speed of 1000 m/s and a misalignment between the atomic beam and a magnetic field of 10^{-3} rad, the motional electric field would be $\sim 1 \text{ mV}/\text{cm}$. However, this misalignment could also be measured and corrected with the same polarization rotation as described above.

The small longitudinal field of $\sim 5 \text{ nV}/\text{cm}$ is justifiable by the means in which this experiment might be performed in practice. For instance, an electric field of each polarity can be applied in the z -direction while conducting phase ramps of the two lasers. From the relative size of the interference signals after changing the applied field polarity, one can accurately measure any additional stray field that might be present, and one can apply a small zeroing field before performing the actual PNC measurement. To combat temporal stray field drifts, these electric field scans can be taken quickly ($\sim \text{Hz}$ level), and a correction made. This would then be followed by a fast PNC measurement. Repeating this process for each PNC measurement scan essentially eliminates long-term temporal drift effects, and short-term drifts will average to zero over many scans.

To demonstrate the effectiveness of this proposed zeroing method, we present an example simulation of what this data collection process may look like. Including the effects of a stray E_z field, we simulated the photon flux exiting the interaction cavity with appropriate shot noise. We emphasize that the electric field contributions to the output flux are orthogonal to that of the weak term, due to the weak matrix element being completely imaginary, while the Stark mixing is real. This effect is shown in the cavity output flux,

$$\Phi_{\text{out}} = \Phi_{\text{in}} \left[\frac{1}{(1-\alpha)^2} - \frac{l}{T(1-\alpha)^3} (\Gamma_w^{(g)} \cos \phi + \Gamma_E^{(g)} \sin \phi) \right], \quad (20)$$

where $\Gamma_E^{(g)}$ is the gain term due to the electric field, and it is equivalent to that of Eq. (13), with the replacement

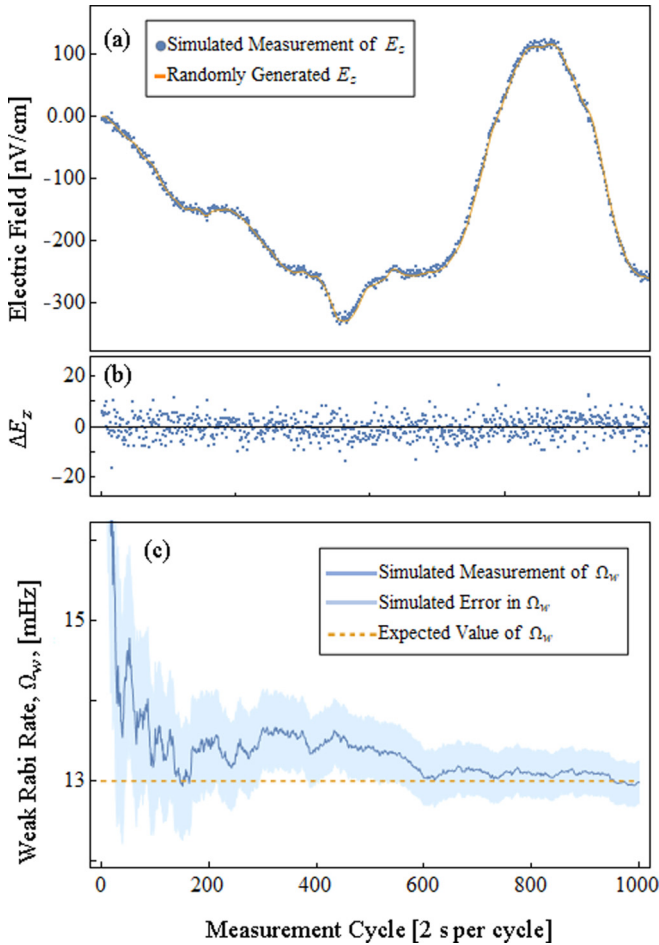


FIG. 6. Simulation results of E_z field zeroing process. (a) Randomly generated E_z field with $1/f^2$ spectral composition along with simulated measurements at each 2 s measurement cycle. (b) The difference between the generated and measured electric field. (c) Simulated measurement of the weak Rabi rate, showing the expected increase in accuracy after averaging over multiple data collection cycles.

$|\Omega_w| \rightarrow \Omega_E$. Aiming for generality, we randomly generate an electric field with $1/f^2$ spectral composition. We perform the measurement in three cycles: first, we apply a large ($1 \mu\text{V}/\text{cm}$) E_z field to our interaction region and perform a 2π phase sweep between our lasers over a $1/2$ s period while integrating the photons exiting our cavity. In a manner similar to evaluating Fourier components, we can extract Γ_E directly by integrating our measured signal multiplied by $\sin \phi$ over the period, which leads to a direct determination of any E_z field present, while ignoring the effects of a cosine term contribution. Then we repeat this measurement cycle while applying a large, negative E_z field to the interaction region. Using these two measurements, the sign and magnitude of any stray field is determined and a correction field is applied. Lastly, with the stray field zeroed, we perform a 1 s PNC measurement. Again, we use the Fourier coefficient methodology to extract Γ_w directly, this time by integrating our signal multiplied by $\cos \phi$, further negating the effects of imperfect E_z field zeroing.

The results of a typical simulation are displayed in Fig. 6. In particular, Fig. 6(a) shows a randomly generated stray E_z field, along with the simulated measurement of this field. For clarity, the difference between the applied field and the measured field is shown in Fig. 6(b), where we note that within our $1/2$ s measurement times we should be able to determine the field at approximately the 5 nV/cm level. For comparison, Merkt and Osterwalder measured an electric field at the $\sim 10 \mu\text{V}/\text{cm}$ level over several hours [36]. Therefore, this implies an upper limit of electric field drift in their apparatus of 1 nV/cm/s. We use this upper bound within our simulation. While the integration time is not sufficient to reduce the stray field to less than 1 nV/cm, and this zeroing method adds shot noise to the E_z field, we want to emphasize that the remaining E_z field should not contaminate the weak measurement. This is for two reasons: the flux signal, as shown in Eq. (20), is linear in E_z , and so contributions average to zero over the course of a long measurement. Additionally, we reiterate the fact that the electric field contributions to our signal are $\pi/2$ out-of-phase with the weak signal, and we are able to distinguish between the two contributors by utilizing Fourier component analysis, a method routinely performed in lock-in amplifiers, for example. This electric field systematic suppression is evident in Fig. 6(c), which shows the extracted weak Rabi rate, Ω_w , for each measurement cycle. The data in this figure are averaged after each new measurement cycle, and we see a clear trend to the expected SM value, with the error decreasing at a rate of $\sqrt{\tau}$. To check for robustness, we ran the simulation using several randomized electric field seeds, and we produced similar results in all cases. Additionally, the sign of the weak interaction can be determined by comparing the relative phase of the weak amplitude to the signal from the parallel or antiparallel applied fields.

3. Low coherent interaction time

An obvious technical challenge introduced in previous hydrogen APV experiments is that, while the $2s$ state is metastable, collisions will induce decays producing a large Lyman- α background. This issue was somewhat avoided in the microwave measurements performed in the mid 1970s to early 1990s by measuring transitions between two metastable $2s$ states. This introduced an atomic coherence time equal to the entire interaction time of the atoms with the microwave fields. The experimental signal was then given by the remaining metastable population after one of the $2s$ states involved in the transition was quenched. This long atomic coherence allowed such measurements to approach SNR_b , but it also puts requirements on the uniformity of the axial magnetic field—interaction times of $1 \mu\text{s}$ require $\Delta B/B \sim 10^{-4}$ over the measurement volume [25].

In the laser-based measurements discussed here, the experimental signal is the power of a visible laser field at 656 nm, so the issue of Lyman- α background is again avoided. However, now the atomic coherence time is given by $\tau_{2p} \approx 1.6$ ns. Therefore, from the perspective of SNR, the requirements on the uniformity of the applied magnetic field are very low and are determined only by the need to drive the $2s$ - $3s$ two-photon transition on resonance.

While increasing the atomic coherence is often beneficial for many precision measurements, we emphasize that this is not the case here. Both the microwave measurements, which require coherent interaction times of 1–1000 μs [25], and the measurement proposed here, which has a coherent interaction time of only 1.6 ns, can approach SNR_b . However, as discussed above, the long coherent interaction time necessary for the microwave measurements introduces stringent requirements on the uniformity of the applied magnetic field.

B. Practical SNR considerations

As is clear from Eq. (6), there are limited ways in which the SNR can be optimized since both Ω_w , and γ_{2p} are fixed properties of atomic hydrogen and $\eta < 1$. Clearly, the most attractive method to increase the SNR is to maximize N_a , the number of metastable atoms within the interaction region. However, as discussed in [25], collision-induced decay from the $|\beta_0\rangle$ state will limit the density to about 3×10^9 at/cm³ if the mean free path is kept to about 30 cm. With a transverse laser beam size of about 1 cm, $N_a \sim 10^9$ should be possible resulting in $\text{SNR}_b \approx 0.1\sqrt{\tau}$. For these rough estimates, a 10% measurement of Ω_w could be achieved with a few hours of integration time.

The flux of metastable $|2\beta_0\rangle$ atoms through the apparatus would need to approach $\sim 10^{15}$ s⁻¹ for the estimates given above. While several methods for achieving this in a thermal beam have been previously proposed [25], here we point out that such metastable production using the 1s-2s transition and a power-scalable and cavity-enhanced 243 nm laser source is a promising possibility. Approximately 100 W in a 1 cm beam, aligned at a small angle to the atomic beam, could be sufficient to excite 1% of the population to the $|2\beta_0\rangle$ state. A recent demonstration of cavity-enhanced 243 nm radiation appears hopeful in this regard [37].

C. Generality of results

As discussed above, we believe this laser-based measurement of APV in hydrogen is competitive in terms of statistical SNR and has distinct advantages when compared with microwave hydrogen APV experiments. We now address how representative this specific scheme is. To elucidate this issue, it is first helpful to note that, all other things being equal,

$$\Omega_w \propto \frac{\sqrt{n^2 - 1}}{n^4}, \quad (21)$$

where n is the principal quantum number [1]. This scaling suggests that 2s-2p level crossings within the $n = 2$ manifold will produce the most sensitive measurements of Ω_w .

With a focus on the hydrogen $n = 2$ manifold, it is apparent given the general considerations in Sec. II that the measurement will ultimately be limited by $A_{\text{pnc}} = 2\Omega_w/\gamma_{2p}$. Therefore, a sensitive measurement should aim to introduce a parity conserving amplitude A_{pc} without degrading A_{pnc} . Applying a magnetic field to make the $|2\beta_0\rangle$ and $|2f_0\rangle$ states degenerate allows the full amplitude A_{pnc} to be realized at $|2f_0\rangle$. To then avoid degrading that amplitude, one can interfere A_{pc} at that state—exactly what our measurement scheme accomplishes.

The precise manner in which A_{pc} is introduced is less important. For instance, three separate dipole-allowed transitions could be driven to move population from $|2\beta_0\rangle$ to $|2f_0\rangle$. This could provide some technical advantage since the power required to drive the first two legs of the transition would be significantly less than that required for the two-photon scheme. For centimeter-scale interaction volumes, ~ 100 W of 1312 nm radiation is required if the two-photon scheme is used. If three dipole-allowed transitions were used, the power requirements would be reduced but the conclusions of Sec. III would remain the same.

For comparison, we have also analyzed the only other laser-based hydrogen APV measurement proposed in the literature—the absorption of 656 nm laser radiation tuned to the transition between $|2\beta_0\rangle$ and $|3\beta_0\rangle$ [26]. This transition can occur because of the weak mixing between $|2\beta_0\rangle$ and $|2f_0\rangle$, which, as in the last example, are made to cross near 1200 G magnetic field. To introduce a parity conserving amplitude, it was suggested to introduce a DC electric field in the y -direction to Stark mix $|2\beta_0\rangle$ with $|2e_1\rangle$ [26]. In this case, a z -polarized field is required to drive the weak-induced $|2f_0\rangle \rightarrow |3\beta_0\rangle$ transition, and an x -polarized field is required to drive the Stark-induced $|2e_1\rangle \rightarrow |3\beta_0\rangle$ transition. The interference at $|3\beta_0\rangle$ will be determined by the relative phase of these two fields, which results in differential absorption for circular polarization of different handedness [$1/\sqrt{2}(\hat{z} \pm i\hat{x})$]. To the best of our knowledge, the SNR for this measurement has never been presented in the literature. The analysis follows that of the previous section, and here we simply quote the result, which is found to be

$$\text{SNR}_a^{\text{cav}} = \text{SNR}_b \frac{\sqrt{2\alpha^{(a)}}}{1 + \alpha^{(a)}} \frac{|\Omega_z^{\text{cav}}|}{\sqrt{\gamma_{2p}\gamma_{3s}}}. \quad (22)$$

Here $\alpha^{(a)}$ is the cavity absorption parameter analogous to $\alpha^{(g)}$ above, and the $\alpha^{(a)}$ -dependent factor has a maximum of $\frac{1}{\sqrt{2}}$ when $\alpha^{(a)} = 1$. The Rabi frequency Ω_z^{cav} is evaluated using the intracavity laser field, which is necessarily much less than $\sqrt{\gamma_{2p}\gamma_{3s}}$ if saturation effects are to be avoided. Overall, this shows that the absorption scheme significantly under-performs compared to the stimulated emission scheme. The lower performance can be easily understood from the arguments above since the interference between A_{pnc} and A_{pc} occurs at $|3\beta_0\rangle$. Therefore, A_{pnc} is degraded by requiring population to be transferred efficiently from $|2f_0\rangle$ to $|3\beta_0\rangle$.

D. Auxiliary experiments

As previously stated, the experimental scheme described here allows a measurement of the linear combination, $C_{1p} + 1.1C_{2p}$, but a similar result can be obtained at the level crossing near 550 G with very little change to the apparatus. The additional measurement at this level crossing between $|2\beta_0\rangle$ and $|2e_0\rangle$ allows for a direct measurement of C_{2p} , and thus allows for both coupling constants to be extracted. A precision measurement of these coupling constants would also lead to a low momentum transfer measurement of the Weinberg mixing angle (described in [7]), potentially testing for dark sector physics.

Thus far, our discussion has focused on hydrogen—although, in practice, measurements would also be conducted in deuterium. A measurement conducted in deuterium would be sensitive primarily to C_{1n} since this is the only electron-nucleon coupling parameter that is not suppressed in the Standard Model (see, for instance, [1,25]). Since C_{1n} is about one order of magnitude larger than C_{1p} and C_{2p} , the same uncertainty can be obtained with about two orders of magnitude less integration time. However, it should be stressed that these measurements provide complementary information.

V. CONCLUSION

APV measurements in hydrogen are compelling due to the unambiguous interpretation of experimental results. Performing a measurement at two level crossings in hydrogen

allows the determination of the weak electron-proton coupling constants, and a similar measurement in deuterium results in the weak electron-neutron coupling constants. The laser-based scheme presented here offers major advantages over microwave experiments, including a short coherent interaction time given by the lifetime of the $2p$ state (1.6 ns), a well-defined interaction volume, and straightforward characterization of systematic effects.

ACKNOWLEDGMENTS

The authors gratefully acknowledge Jacob Roberts and Samuel Brewer for both helpful discussions and reviewing this manuscript. This material is based upon work supported by the National Science Foundation Graduate Research Fellowship Program under Grant No. 000202-00067.

-
- [1] G. W. F. Drake, Theory of transitions, and the electroweak interaction, in *The Spectrum of Atomic Hydrogen: Advances* (World Scientific, Singapore, 1988).
- [2] K. Abe *et al.* (SLD Collaboration), High-Precision Measurement of the Left-Right Z Boson Cross-Section Asymmetry, *Phys. Rev. Lett.* **84**, 5945 (2000).
- [3] G. P. Zeller, K. S. McFarland, T. Adams, A. Alton, S. Avvakumov, L. de Barbaro, P. de Barbaro, R. H. Bernstein, A. Bodek, T. Bolton *et al.* (NuTeV Collaboration), Precise Determination of Electroweak Parameters in Neutrino-Nucleon Scattering, *Phys. Rev. Lett.* **88**, 091802 (2002).
- [4] P. L. Anthony *et al.* (SLAC E158 Collaboration), Precision Measurement of the Weak Mixing Angle in Møller Scattering, *Phys. Rev. Lett.* **95**, 081601 (2005).
- [5] D. Androić *et al.* (The Jefferson Lab Qweak Collaboration), Precision measurement of the weak charge of the proton, *Nature (London)* **557**, 207 (2018).
- [6] S. G. Porsev, K. Beloy, and A. Derevianko, Precision Determination of Electroweak Coupling from Atomic Parity Violation and Implications for Particle Physics, *Phys. Rev. Lett.* **102**, 181601 (2009).
- [7] H. Davoudiasl, H.-S. Lee, and W. J. Marciano, Low Q^2 weak mixing angle measurements and rare Higgs decay, *Phys. Rev. D* **92**, 055005 (2015).
- [8] M. A. Bouchiat and C. C. Bouchiat, Weak neutral currents in atomic physics, *Phys. Lett. B* **48**, 111 (1974).
- [9] M. J. D. Macpherson, K. P. Zetie, R. B. Warrington, D. N. Stacey, and J. P. Hoare, Precise Measurement of Parity Nonconserving Optical Rotation at 876 nm in Atomic Bismuth, *Phys. Rev. Lett.* **67**, 2784 (1991).
- [10] D. M. Meekhof, P. A. Vetter, P. K. Majumder, S. K. Lamoreaux, and E. N. Fortson, High-Precision Measurement of Parity Non-Conserving Optical Rotation in Atomic Lead, *Phys. Rev. Lett.* **71**, 3442 (1993).
- [11] R. B. Warrington, C. D. Thompson, and D. N. Stacey, A new measurement of parity-non-conserving optical rotation at 648 nm in atomic bismuth, *Europhys. Lett.* **24**, 641 (1993).
- [12] N. H. Edwards, S. J. Phipp, P. E. G. Baird, and S. Nakayama, Precise Measurement of Parity Nonconserving Optical Rotation in Atomic Thallium, *Phys. Rev. Lett.* **74**, 2654 (1995).
- [13] P. A. Vetter, D. M. Meekhof, P. K. Majumder, S. K. Lamoreaux, and E. N. Fortson, Precise Test of Electroweak Theory from a New Measurement of Parity Nonconservation in Atomic Thallium, *Phys. Rev. Lett.* **74**, 2658 (1995).
- [14] S. J. Phipp, N. H. Edwards, P. E. G. Baird, and S. Nakayama, A measurement of parity non-conserving optical rotation in atomic lead, *J. Phys. B* **29**, 1861 (1996).
- [15] C. S. Wood, S. C. Bennett, D. Cho, B. P. Masterson, J. L. Roberts, C. E. Tanner, and C. E. Wieman, Measurement of parity non-conservation and an anapole moment in cesium, *Science* **275**, 1759 (1997).
- [16] M. Lintz, J. Guena, and M. A. Bouchiat, Pump-probe measurement of atomic parity violation in cesium with a precision of 2.6%, *Eur. Phys. J. A* **32**, 525 (2007).
- [17] K. Tsigtukin, D. Dounas-Frazer, A. Family, J. E. Stalnaker, V. V. Yashchuk, and D. Budker, Observation of a Large Atomic Parity Violation Effect in Ytterbium, *Phys. Rev. Lett.* **103**, 071601 (2009).
- [18] D. Antypas, A. Fabricant, J. E. Stalnaker, K. Tsigtukin, V. V. Flambaum, and D. Budker, Isotopic variation of parity violation in atomic ytterbium, *Nat. Phys.* **15**, 120 (2019).
- [19] S. G. Porsev, K. Beloy, and A. Derevianko, Precision determination of weak charge of ^{133}Cs from atomic parity violation, *Phys. Rev. D* **82**, 036008 (2010).
- [20] Ya. B. Zel'dovich, Parity nonconservation in the first order in the weak interaction constant in electron scattering and other effects, *Sov. Phys. JETP* **9**, 682 (1959).
- [21] F. Curtis Michel, Neutral weak interaction currents, *Phys. Rev.* **138**, B408 (1965).
- [22] R. W. Dunford, R. R. Lewis, and W. L. Williams, Parity non-conservation in the hydrogen atom. II, *Phys. Rev. A* **18**, 2421 (1978).
- [23] E. A. Hinds, Sensitivity and the Role of Level Crossings in Measurements of Parity Nonconservation Using Metastable Atoms, *Phys. Rev. Lett.* **44**, 374 (1980).
- [24] E. N. Fortson and L. L. Lewis, Atomic parity nonconservation experiments, *Phys. Rep.* **113**, 289 (1984).

- [25] R. W. Dunford and R. J. Holt, Parity violation in hydrogen revisited, *J. Phys. G* **34**, 2099 (2007).
- [26] R. R. Lewis and W. L. Williams, Parity nonconservation in the hydrogen atom, *Phys. Lett. B* **59**, 70 (1975).
- [27] W. E. Lamb Jr. and R. C. Retherford, Fine structure of the hydrogen atom, Part I, *Phys. Rev.* **79**, 549 (1950).
- [28] M. Haas, U. D. Jentschura, C. H. Keitel, N. Kolachevsky, M. Herrmann, P. Fendel, M. Fischer, Th. Udem, R. Holzwarth, T. W. Hänsch, M. O. Scully, and G. S. Agarwal, Two-photon excitation dynamics in bound two-body Coulomb systems including ac Stark shift and ionization, *Phys. Rev. A* **73**, 052501 (2006).
- [29] D. Antypas and D. S. Elliott, Measurement of weak optical transition moments through two-pathway coherent control, *Can. J. Chem.* **92**, 144 (2014).
- [30] D. A. Steck, Quantum and atom optics, available online at <http://steck.us/teaching> (revision 0.12.2, 11 April 2018).
- [31] J. Verdeyen, *Laser Electronics*, 3rd ed. (Pearson Prentice Hall, Upper Saddle River, NJ, 2000), p. 642.
- [32] J. Verdeyen, *Laser Electronics*, 3rd ed. (Pearson Prentice Hall, Upper Saddle River, NJ, 2000), p. 593.
- [33] C. C. W. Fehrenbach, An experimental limit on parity mixing in atomic hydrogen, Ph.D. dissertation, University of Michigan, 1993.
- [34] M. Z. Iqbal, A search for parity-nonconservation in the hydrogen atom, Ph.D. dissertation, University of Washington, 1983.
- [35] J. M. Hettema, Upper bound on parity nonconservation in 2S hydrogen, Ph.D. dissertation, Yale University, 1990.
- [36] A. Osterwalder and F. Merkt, Using High Rydberg States as Electric Field Sensors, *Phys. Rev. Lett.* **82**, 1831 (1999).
- [37] S. F. Cooper, Z. Burkley, A. D. Brandt, C. Rasor, and D. C. Yost, Cavity-enhanced deep ultraviolet laser for two-photon cooling of atomic hydrogen, *Opt. Lett.* **43**, 1375 (2018).